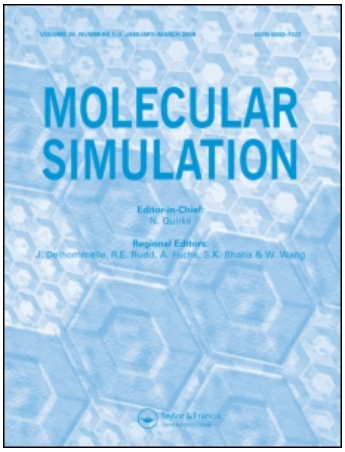

Molecular Simulation

Publication details, including instructions for authors and subscription information:
http://www.informaworld.com/smpp/title~content=t713644482

Molecular dynamics simulations to investigate the stability and aggregation behaviour of the amyloid-forming peptide VQIVYK from tau protein

Jian-Hua Zhao[a]; Hsuan-Liang Liu[ab]; Chih-Kuang Chuang[bcd]; Kung-Tien Liu[e]; Wei-Bor Tsai[f]; Yih Ho[g]
[a] Department of Chemical Engineering and Biotechnology, National Taipei University of Technology, Taipei, Taiwan, R.O.C. [b] Graduate Institute of Biotechnology, National Taipei University of Technology, Taipei, Taiwan, R.O.C. [c] Division of Genetics and Metabolism, Department of Medical Research, Mackay Memorial Hospital, Taipei, Taiwan, R.O.C. [d] College of Medicine, Fu-Jen Catholic University, Taipei County, Taiwan, R.O.C. [e] Chemical Analysis Division, Institute of Nuclear Energy Research, Taoyuan County, Taiwan, R.O.C. [f] Department of Chemical Engineering, National Taiwan University, Taipei, Taiwan, R.O.C. [g] School of Pharmacy, Taipei Medical University, Taipei, Taiwan, R.O.C.

Online publication date: 24 November 2010

To cite this Article Zhao, Jian-Hua , Liu, Hsuan-Liang , Chuang, Chih-Kuang , Liu, Kung-Tien , Tsai, Wei-Bor and Ho, Yih(2010) 'Molecular dynamics simulations to investigate the stability and aggregation behaviour of the amyloid-forming peptide VQIVYK from tau protein', Molecular Simulation, 36: 13, 1013 — 1024
To link to this Article: DOI: 10.1080/08927022.2010.499147
URL: http://dx.doi.org/10.1080/08927022.2010.499147

Molecular Simulation
Vol. 36, No. 13, November 2010, 1013–1024

Taylor & Francis
Taylor & Francis Group

Molecular dynamics simulations to investigate the stability and aggregation behaviour of the amyloid-forming peptide VQIVYK from tau protein

Jian-Hua Zhao[a], Hsuan-Liang Liu[ab]*, Chih-Kuang Chuang[bcd], Kung-Tien Liu[e], Wei-Bor Tsai[f] and Yih Ho[g]

[a]*Department of Chemical Engineering and Biotechnology, National Taipei University of Technology, 1 Section 3 Zhong Xiao East Road, Taipei 10608, Taiwan, R.O.C.;* [b]*Graduate Institute of Biotechnology, National Taipei University of Technology, 1 Section 3 Zhong Xiao East Road, Taipei 10608, Taiwan, R.O.C.;* [c]*Division of Genetics and Metabolism, Department of Medical Research, Mackay Memorial Hospital, 92, Section 2, Chung-Shan North Road, Taipei 10449, Taiwan, R.O.C.;* [d]*College of Medicine, Fu-Jen Catholic University, 510 Chung Cheng Road, Hsinchuang, Taipei County 24205, Taiwan, R.O.C.;* [e]*Chemical Analysis Division, Institute of Nuclear Energy Research, 1000, Wunhua Road, Longtan Township, Taoyuan County 32546, Taiwan, R.O.C.;* [f]*Department of Chemical Engineering, National Taiwan University, 1 Section 4 Roosevelt Road, Taipei 106, Taiwan, R.O.C.;* [g]*School of Pharmacy, Taipei Medical University, 250 Wu-Hsing Street, Taipei 110, Taiwan, R.O.C.*

(*Received 17 September 2009; final version received 2 June 2010*)

The formation of paired helical filaments arising from the short hexapeptide in the third repeat of tau protein, ^{306}VQIVYK^{311}, is critical for tau polymerisation. The atomic structure of the VQIVYK oligomer has revealed a dry, tightly self-complementing structure between the neighbouring β-sheet layers, termed as 'steric zipper'. In this study, several molecular dynamics simulations with all-atom explicit water were conducted to investigate the structural stability and aggregation behaviour of the VQIVYK peptide with various sizes and its single alanine replacement mutations. Our results indicate that the van der Waals interaction between side chains of Q2, the π−π stacking interaction between aromatic rings of Y5, and the electrostatic interaction between K6 and the C-terminus play an important role in stabilising the VQIVYK oligomers within the same β-sheet layer, while hydrophobic steric zipper involving V1, I3 and Y5 is responsible for holding the neighbouring β-sheet layers together. The twisted angles of the VQIVYK oligomers were also analysed and shown to be size dependent. The present results not only provide atomic insights into amyloid formation, but are also helpful for designing new or modified capping peptides and inhibitors to prevent fibril formation of the VQIVYK peptide from tau protein.

Keywords: VQIVYK peptide; tau protein; steric zipper; molecular dynamics simulations; π−π stacking interaction

1. Introduction

The senile plaques or neurofibrillary tangles (NFTs), formed by fibrous assemblies of the Aβ peptide or tau protein, have become characteristic hallmarks of a definitive diagnosis of Alzheimer's disease after the patient's death [1]. These insoluble aggregates are thought to be toxic to neurons either by causing toxic signalling defect or by obstructing the cell interior. The precipitation of NFTs in the cytoplasm is attributed to the fact that the ordered cytoskeleton consisting of microtubules, tau and intermediate filaments is destroyed. The major constituents of NFTs are paired helical filaments (PHFs) and straight filaments [2]. The hyperphosphorylated tau, the major component for insoluble PHFs, has been proposed to play an important role in dissociating tau and tubulin [3–5].

Tau protein is one of the neuronal microtubule-associated proteins and contributes to stabilise an axonal microtubule. Although it exhibits an unfolded flexible structure dominated by a random-coil conformation in aqueous solution [6–8], tau undergoes a structural transition from unfolded structures to well-defined fibres, the PHFs [9]. The core of tau aggregation is mainly involved in the microtubule-binding domain (MBD), which is composed of three or four repeats of 31 or 32 amino acids [10]. MBD also exhibits seeding effects on the PHF assembly *in vitro* [11,12]. It has been hypothesised that the formation of the β-sheet structure arising from the short hexapeptide in the second and third repeats of tau, ^{275}VQIINK^{280} (PHF6* in R2) and ^{306}VQIVYK^{311} (PHF6 in R3) [13–16], is critical for tau polymerisation. It has also been speculated that the interaction between these two regions gives rise to the unique PHF morphology [13,14]. Recent experimental results have indicated that the tripeptide VYK is minimally sufficient for fibril formation and that mixing VYK with PHF6 can form PHF-like twisted filaments [17]. However, the initial oligomerisation process of the full-length tau protein or the peptide fragments has still remained unclear so far.

It is believed that the protein/peptide fibril formation and deposition share common pathogenic mechanisms. Experimental evidences have led to the commonly accepted notion that a cross-β-spine represents the basic structural motif of amyloid fibres [18,19]. Nevertheless, the complete structural definition of these aggregates is still

*Corresponding author. Email: f10894@ntut.edu.tw

ISSN 0892-7022 print/ISSN 1029-0435 online

DOI: 10.1080/08927022.2010.499147
http://www.informaworld.com

highly debated. Over the years, several structural models, essentially variations on a common theme (cross-β-spine), have been proposed [20]. In addition, the fibres can be stained with dyes that interact preferentially with β-sheets, such as Congo Red, thioflavine S and others. These findings together reveal that a general principle may govern amyloid fibril formation [21]. Recent advances have revealed a common 'steric zipper' motif, in which pairs of β-sheet layers form a dry interface with interdigitation of side chains [22,23], which provides insights into understanding the structure, mechanisms and disease association of amyloidogenic peptides [22,23]. Among these steric zipper structures, the structural characterisation of the VQIVYK peptide from tau protein reveals a parallel β-strand orientation within the same β-sheet layer with an antiparallel organisation between the two neighbouring β-sheet layers (Figure 1(a)).

Understanding the dynamic behaviours of the amyloidogenic peptides is expected to provide insights into the possible mechanism of amyloid formation. Molecular dynamics (MD) simulations have become a useful tool to offer unique opportunities to observe and analyse the early aggregation events at the molecular level [24–39]. In this study, several extensive full atomistic MD simulations of the VQIVYK oligomers with various sizes and their single alanine mutations were conducted to investigate: (i) the influence of the number of the VQIVYK peptide on the structural stability and conformational dynamics of the VQIVYK oligomers; (ii) the principle driving force to associate or initialise the VQIVYK aggregation; (iii) the role of the hydrophobic steric zipper on the stabilisation and association of the VQIVYK aggregates; (iv) the effects of single alanine mutation on the structural stability of the VQIVYK oligomer; and (v) the twisted phenomenon of the β-strands within the same β-sheet layer of the VQIVYK oligomers.

2. Method

2.1 Model building

The microcrystal structure of the VQIVYK assembly has been determined by Sawaya et al. [23], available at http://www.doe-mbi.ucla.edu/ ~ sawaya/chime/xtalpept/. The Biopolymer module of the InsightII program (Accelrys, San Diego, CA, USA) was used to construct the oligomeric models of the VQIVYK peptide with different sizes. For the wild-type systems, the one-sheet models consisted of two-, three-, four- and five-parallel strands, respectively. The two-sheet models consisted of two-, three-, four- and five-parallel strands within the same β-sheet layers while maintaining antiparallel organisation between the neighbouring β-sheet layers (Figure 1(b)). For the mutant systems, six single-point Ala mutations were constructed, termed as V1A, Q2A, I3A, V4A, Y5A and K6A, based on the wild-type SH2-ST5 model. The detailed simulation conditions for each model are summarised in Table 1.

2.2 Simulation protocol

Molecular minimisation and MD simulations were carried out using Discover3 in InsightII program with the consistent valence force field. The BIOPOLYMER module of InsightII was used to add hydrogen atoms to mimic the neutral pH condition [23]. After initial minimisation with the steepest descent method for 5000 iterations and conjugated gradient method for 5000 iterations, each of these structural models was then placed in a cell with at least 10 Å from the edge of the protein and soaked with water molecules using Assemble module of the InsightII program. To further optimise the arrangement of the solvent molecules around the VQIVYK oligomers and alleviate high energy regions, solvent molecules alone were allowed to relax by running a short 200 ps MD simulation with position restraints applied to all the VQIVYK oligomer atoms. Subsequently, the VQIVYK

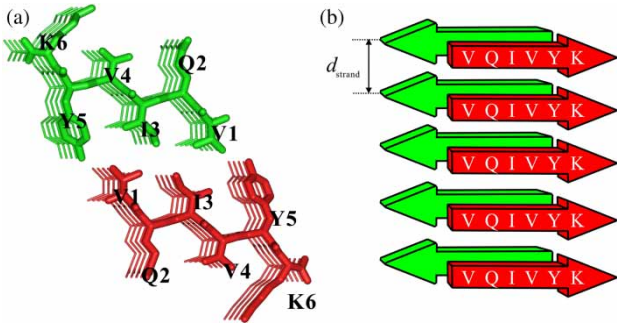

Figure 1. (a) Top view of the atomistic representation of the SH2-ST5 model of the VQIVYK oligomers and (b) side view of the schematic organisation of the VQIVYK oligomer. β-Sheet layers 1 and 2 are coloured in green and red, respectively (colour online). Hydrogen atoms are deleted for clarity. The interstrand distance (d_{strand}) is also indicated.

Table 1. Summary of the VQIVYK oligomeric models and their simulation conditions.

Label	System	Strand/sheet organisation	Simulation box size (Å)
Wild-type			
SH1-ST2	1 Sheet, 2 strands	Parallel/–	38 × 28 × 30
SH1-ST3	1 Sheet, 3 strands	Parallel/–	38 × 33 × 30
SH1-ST4	1 Sheet, 4 strands	Parallel/–	38 × 38 × 30
SH1-ST5	1 Sheet, 5 strands	Parallel/–	38 × 43 × 30
SH2-ST2	2 Sheet, 2 strands	Parallel/antiparallel	55 × 30 × 38
SH2-ST3	2 Sheet, 3 strands	Parallel/antiparallel	55 × 36 × 38
SH2-ST4	2 Sheet, 4 strands	Parallel/antiparallel	55 × 42 × 38
SH2-ST5	2 Sheet, 5 strands	Parallel/antiparallel	55 × 48 × 38
Mutants			
V1A	2 Sheet, 5 strands, V1A	Parallel/antiparallel	55 × 48 × 38
Q2A	2 Sheet, 5 strands, Q2A	Parallel/antiparallel	55 × 48 × 38
I3A	2 Sheet, 5 strands, I3A	Parallel/antiparallel	55 × 48 × 38
V4A	2 Sheet, 5 strands, V4A	Parallel/antiparallel	55 × 48 × 38
Y5A	2 Sheet, 5 strands, Y5A	Parallel/antiparallel	55 × 48 × 38
K6A	2 Sheet, 5 strands, K6A	Parallel/antiparallel	55 × 48 × 38

oligomers alone were minimised with 5000 steps, followed by the minimisation of the entire system for additional 5000 iterations. The system was energy-minimised with the method described above until the maximum derivative was lower than 0.001 kcal mol^{-1} Å^{-1}. Finally, 20 ns MD simulation for each model was carried out with constant temperature constraint at 330 K. This simulation temperature is slightly higher than room temperature to avoid kinetic traps and allows us to probe the stabilities and dynamics of the VQIVYK oligomers more quickly in the limited simulation time scale. The time step for integration was 2 fs using the Rattle algorithm to constrain the bonds connecting hydrogen atoms during simulation [40]. A cut-off radius of 12 Å for both non-bonded electrostatic and van der Waals interactions was employed. The trajectories were saved every 1 ps for further structural analyses using Analysis and Measure module of the InsightII program.

2.3 Structural analyses

The interstrand distance (d_{strand}) was calculated by averaging pairwise residue C_α–C_α distances of V1–V1, Q2–Q2, I3–I3, V4–V4, Y5–Y5 and K6–K6 within the same β-sheet layer. [34]. A side-chain contact was assigned when the distance between the centres of mass (COM) of two adjacent side chains was less than 6.7 Å [41]. Two charged groups were considered to interact when the distance between their interaction centres, i.e. the carbon atom of the C-terminus or the charged nitrogen atom of Lys, was 4.5 Å or less [42,43]. The aromatic–aromatic interaction was counted when the distance between two ring centroids (d) was less than 7.5 Å [44]. To further analyse the various geometric orientations of the aromatic–aromatic interactions, the other two parameters (P and θ) were calculated, as shown in Figure 2. In addition, to evaluate the structural compactness of the hydrophobic steric zipper involving V1, I3 and Y5, the radius of gyration (R_g) of their side chains was calculated using the Insight II program. The difference of R_g was defined as $\Delta R_g = R_{gi} - R_{g0}$, where R_{gi} and R_{g0} are the R_g of the hydrophobic side chains of V1, I3 and Y5 during the simulation and in the crystal structure, respectively. The twisted angle was defined as the angle between the vector C_α(Q2)–C_α(Y5) and vector C_α(Q2)–C_α(Y5) of two adjacent β-strands within the same β-sheet layer.

3. Results and discussion

3.1 The relative structural stability of the VQIVYK oligomers with different sizes

3.1.1 One-sheet models

The time series of the interstrand distance (d_{strand}) of the VQIVYK oligomers with various sizes are plotted in Figure 3 to indicate their relative stabilities. As shown in Figure 3(a), the d_{strand} of the SH1-ST2 model increased sharply at 5 ns and reached to the value of 12 Å after 7.5 ns, indicating that the SH1-ST2 model lost most of its structural integrity during the simulation. Similarly, the d_{strand} of the SH1-ST3 model increased sharply at 5 ns and reached to equilibrium value of nearly 10 Å, suggesting that the SH1-ST3 model partially lost its structural organisation to a less extent than the SH1-ST2 model. In contrast, the SH1-SH5 model maintained its structural integrity well with remarkably low values of d_{strand}. For SH1-ST4, the magnitudes of the d_{strand} fluctuations are between those of the SH1-ST2 and SH1-ST5 models. These results indicate that the structural stability of the VQIVYK oligomers increases with increasing the number of β-strands for the one-sheet models, which is consistent with the previous MD study of the human calcitonin-derived peptide DFNKF (hCT15-19), showing that the

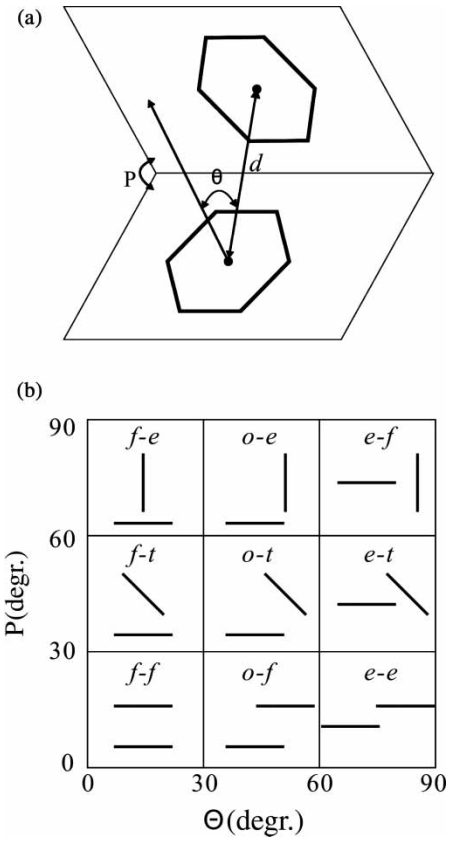

Figure 2. (a) Three parameters (d, P and θ) used to investigate the aromatic–aromatic interactions; d is the distance between the side-chain centroids, P the interplanar angle between two rings, and θ the angle between the line joining the centroids of the two interacting aromatic rings and the normal to the plane of the reference ring. (b) Various geometric orientations of the aromatic–aromatic interactions in accordance with different combinations of P and θ. On the basis of the two angles, nine different geometric orientations of the interacting rings can be distinguished, which are indicated by two letters: f–f, o–f, e–e, f–t, o–t, e–t, f–e, o–e and e–f. The first letter relates to the reference residue and shows whether this ring interacts with its face (f) or edge (e), or the centroid of the second ring is in an offset (o) position. The second letter relates to the second ring in the interacting pair and shows whether this ring is tilted (t) relative to the reference ring, or takes part in the aromatic–aromatic interaction with its face (f) or edge (e).

stability of the DFNKF oligomers increases with their sizes [34]. Theoretical studies of the amyloidogenic peptide GNNQQNY [45] and the GGVVIA peptide [39] also suggested that the stability of these oligomers increases with increasing the number of β-strands. Thus, we suggest that an extra β-strand facilitates the aggregation process of these peptides, a sequence-independent behaviour.

3.1.2 *Two-sheet models*

In Figure 3(a), d_{strand} of the SH2-ST2 model exhibits large fluctuations within 5 ns and then increases quickly

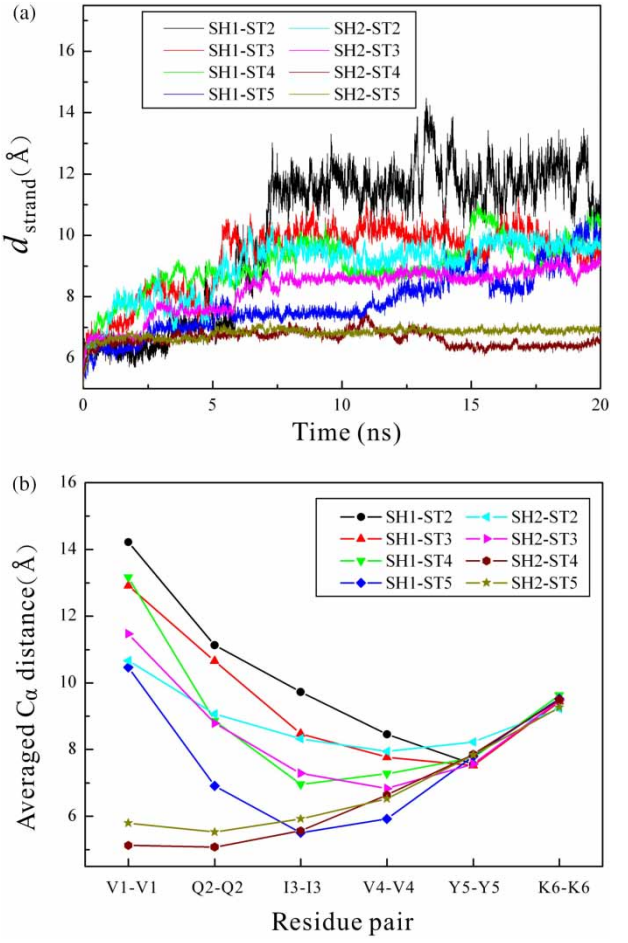

Figure 3. (a) Interstrand distance (d_{strand}) and (b) averaged pairwise residue C_α–C_α distances of the wild-type models during the 20 ns MD simulations.

to 10 Å after 8 ns. The SH2-ST3 model is more stable than the SH2-ST2 model due to the relative low d_{strand} during the entire simulation courses. It is observed that d_{strand} of both SH2-ST4 and SH2-ST5 models are well preserved to the equilibrium values of nearly 6.8 Å during most of the simulation courses, indicating that these two models exhibit higher ability to maintain their structural stability than the SH2-ST2 and SH2-ST3 models. Similar to the one-sheet models, the structural stability of the VQIVYK oligomers also increases with increasing the number of β-strands for the two-sheet models. A recent Monte Carlo study has reported that the aggregation size of a stable two-sheet aggregate for tau fragment AcPHF6 (Ac-VQIVYK-NH2) is 11, whereas aggregates with $\leqq 7$ chains are quite rare [46]. Our simulation results show that the SH2-ST4 (eight chains) and SH2-ST5 (10 chains) models are remarkably stable during the entire simulation courses, whereas the SH2-ST2 (four chains) and SH2-ST3 (six chains) models are relatively unstable, and are consistent with the theoretical

results of Li et al. [46]. To ensure the reproducibility of the present simulation results, additional MD simulation runs for the SH2-ST4 and SH2-ST5 models were also performed and the results are comparable with those of the original runs (data not shown). It further indicates that the results from single trajectories might be sufficient to establish the conclusion that the SH2-ST4 and SH2-ST5 models are the most stable models examined in this study.

3.1.3 Comparison between one- and two-sheet models

Comparisons between the one- and two-sheet models suggest that an extra β-sheet layer significantly increases the entire oligomeric stability of the VQIVYK oligomers. It can be attributed to the fact that an extra β-sheet layer decreases the exposure of peptides to the solvent [45] and provides additional sheet–sheet interactions to associate the strands. Our results are also in good agreement with the pervious theoretical results, showing that higher-order oligomers do not dissociate quickly due to their small diffusion coefficients and slow kinetics [34,39,45].

3.2 The role of side-chain interactions on the structural stability of VQIVYK oligomers

3.2.1 The van der Waals interaction of Glu2

To further explore the structural stability of the VQIVYK oligomers with various sizes, the averaged pairwise C_α–C_α distances were calculated and the results are plotted in Figure 3(b). It is obvious that the pairwise C_α–C_α distances for V1–V1 and Q2–Q2 decrease with increasing the number of strands for both one- and two-sheet models. Previously, the polar residues, such as Gln and Asn, have been shown to play an important role in stabilising the β-sheet amyloid-like aggregates of the GNNQQNY peptide through van der Waals interactions [45]. In order to examine the effect of the similar interaction between Q2 on the structural stability of the VQIVYK aggregates, the COM distance (d_{COM}) between the side chains of Q2 against the interstrand distance (d_{strand}) are depicted in Figure 4. A positive and linear correlation was found for both one- and two-sheet models, indicating that the van der Waals interactions between Q2 side chains contribute to the structural stability of the VQIVYK oligomers, resulting in relatively low pairwise C_α–C_α distances for V1–V1 and Q2–Q2, as observed in Figure 3(b).

3.2.2 The π–π stacking interactions of Tyr5

In contrast to V1–V1 and Q2–Q2 pairs, the averaged pairwise C_α–C_α distances for Y5–Y5 and K6–K6 are

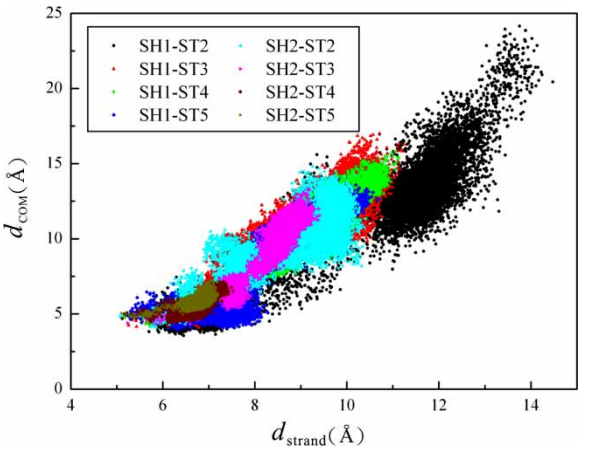

Figure 4. Plots of the interstrand distance (d_{strand}) against the COM distances (d_{COM}) of the side chain between Q2–Q2 pairs in the wild-type models during the 20 ns MD simulations.

conserved for both one- and two-sheet models, which can be attributed to the π–π stacking interactions between the aromatic rings of Y5. To further explore the role of the π–π stacking interactions between Y5 on the structural stability of the VQIVYK oligomers, the distribution of the d_{COM} between the Y5 aromatic rings was calculated and the results are shown in Figure 5(a). It is observed that the highest peak of the distribution is around 5–6 Å, which is consistent with the previous statistic study, showing that the centroid–centroid separation of aromatic side-chain pairs exhibits a relative high peak at 5–6 Å. Our results show that the π–π stacking interactions between the Y5 aromatic rings are well preserved during most of the simulation courses for both one- and two-sheet models. It is of interest to further investigate the π–π stacking arrangements between the Y5 aromatic rings of the VQIVYK oligomers. The relative spatial orientations of the interacting aromatic rings were characterised on the basis of the two parameters (P and θ), as described by Bhattacharyya et al. [47]. Various types of aromatic–aromatic interactions were classified in accordance with different combinations of P and θ (Figure 2(b)) and the results are presented in Figure 6. It is obvious that the Y5 aromatic rings do not adopt the face-to-face π–π stacking arrangement as observed in the crystal structures (Figure 1). Instead, the preferred orientations are offset-to-edge (o–e), offset-to-tilt (o–t), edge-to-face (e–f) and edge-to-tilt (e–t). It can be attributed to the twisted β-strand organisation, which optimises the π–π stacking of the Y5 aromatic rings between the adjacent β-strands, resulting in the disappearance of the face-to-face π–π stacking arrangement.

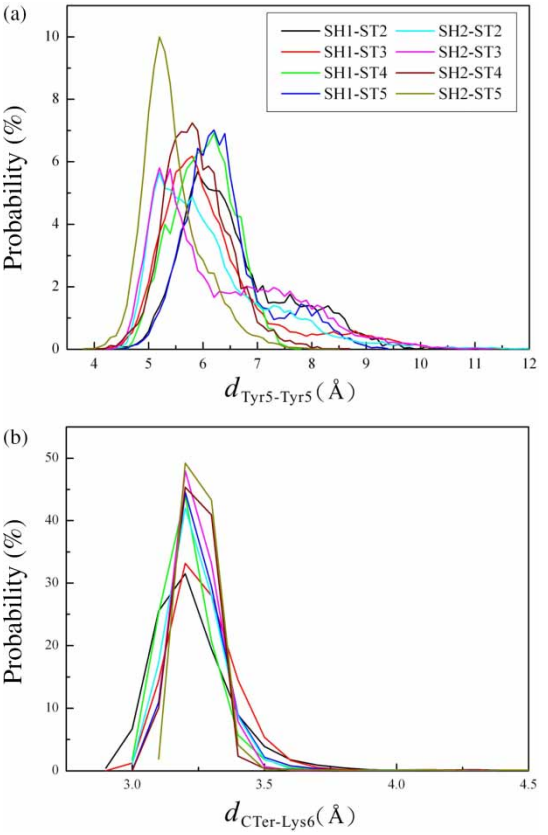

Figure 5. Distributions of (a) the COM distances of aromatic rings of Y5 between the adjacent β-strands and (b) the distance between the charged nitrogen atom of the side chain of K6 and the carbon atom of the C-terminus in the wild-type models.

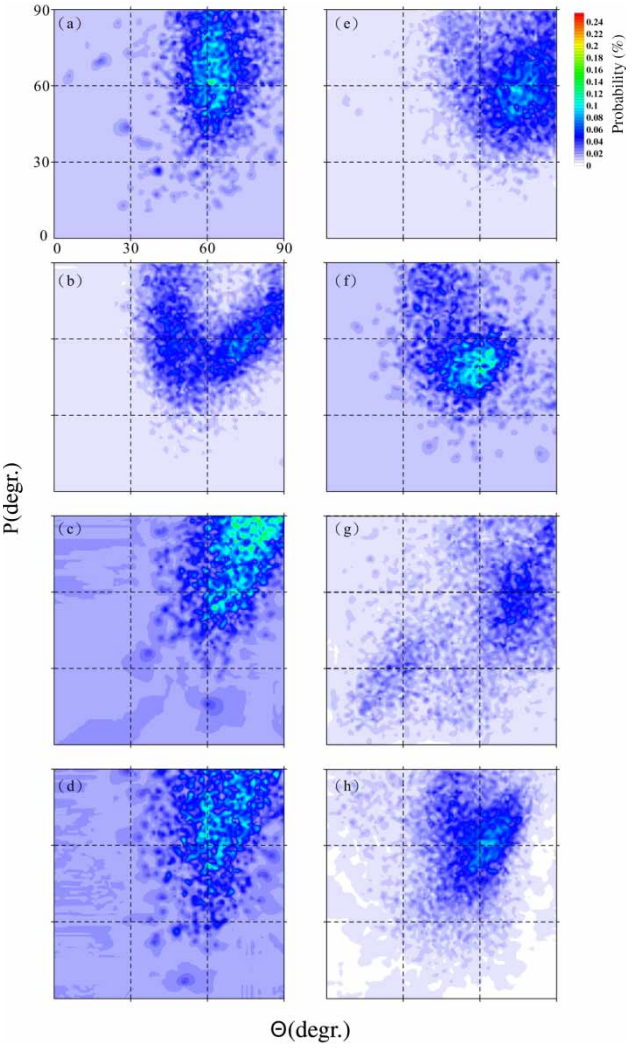

Figure 6. Contour maps between the angles P and θ in the (a) SH1-ST2, (b) SH1-ST3, (c) SH1-ST4, (d) SH1-ST5, (e) SH2-ST2, (f) SH2-ST3, (g) SH2-ST4 and (h) SH2-ST5 models.

3.2.3 The electrostatic interaction between Lys6 and C-terminus

Similar to the Y5–Y5 pair, the averaged pairwise C_α–C_α distance for K6–K6 is also conserved at 9.5 Å for both one- and two-sheet models (Figure 3(b)). Previous MD study of the amyloid fibril formation for the DFNKF peptide from the human calcitonin hormone has indicated that the electrostatic interactions between Lys and the C-terminus and between Asp and the N-terminus are the most important interactions contributing to the stability of the DFNKF organisation [34,35,48]. Similar electrostatic interaction between K6 and the C-terminus was also found for the VQIVYK oligomers. The distributions of the distances between the charged nitrogen atom of the K6 side chain and the carbon atom of the C-terminus were computed and the results are shown in Figure 5(b). It exhibits a narrow peak around 3.5–4.5 Å, suggesting that the electrostatic interactions between K6 and C-terminus are almost preserved during the entire simulation course, leading to the association of the adjacent β-strands.

3.2.4 Y5 and K6 play critical role in initiating VQIVYK aggregation

Figure 7(a) and (b) shows the snapshots of the SH1-ST2 and SH1-ST3 models at 20 ns, respectively, which mimic the early stage of VQIVYK aggregation. These structures show that the π–π stacking interactions between the Y5 aromatic rings and the electrostatic interactions between K6 and C-terminus are well preserved, indicating that these interactions play a critical role in initiating the aggregation of the VQIVYK peptide. In contrast, the van der Waals interaction of Q2 is not strong enough to associate the β-strands, resulting in the N-terminal dissociation of the VQIVYK peptide. Taken together, our results strongly suggest that Y5 and K6 may participate in the core nucleation site at the early stage of VQIVYK aggregation. Our results are supported by the previous experimental observations where the tripeptide

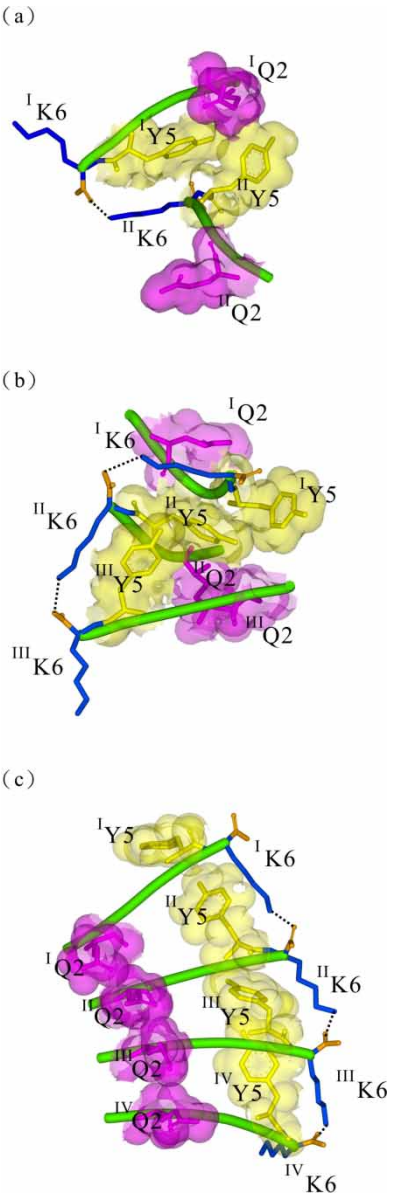

Figure 7. Snapshots of the (a) SH1-ST2, (b) SH1-ST3 and (c) SH2-ST4 models at 20 ns. First, second, third and fourth β-strands are denoted as I, II, III and IV, respectively. The van der Waals surfaces for the side chains of the Q2 and Y5 residues are coloured in magenta and yellow, respectively. The side chain of K6 and C-terminus are coloured in blue and orange, respectively (colour online). The β-sheet layer 2 was deleted for clarity in the SH2-ST4 model.

VYK acts as the core nucleation site for the formation of amyloid fibrils displaying the PHF morphology characteristic of NFTs [17]. Nevertheless, the van der Waals interactions of Q2 can be further enhanced with increasing the oligomeric sizes and thus contribute positively to the entire oligomeric structures of higher-order oligomers, such as the SH2-ST4 and SH2-ST5 models (Figure 7(c)).

3.3 *Stabilising interactions between β-sheet layers*

Early results of this study show that the two-sheet models exhibit higher ability to preserve the structural integrity of the VOIVYK oligomers than the one-sheet models (Figure 3(a) and (b)). Moreover, V1, I3 and Y5 are pointed towards the interface to form a hydrophobic steric zipper between the two neighbouring β-sheet layers as observed in the crystal structure of the VQIVYK oligomers [23]. To evaluate the compactness of the hydrophobic steric zipper involving V1, I3 and Y5, the radius of gyration (R_g) of their side chains was calculated using the Insight II program. The difference in their R_g (ΔR_g) was calculated and the results are presented in Figure 8. It shows that the SH2-ST2 and SH2-ST3 models exhibit high peaks of ΔR_g between the range of 1–1.5 Å, whereas the highest peaks of ΔR_g are around 0 Å for both SH2-ST4 and SH2-ST5 models, indicating that the hydrophobic steric zipper is well preserved in higher-ordered two-sheet models.

In order to illustrate the correlation between the structural stability and the intersheet hydrophobic steric zipper involving V1, I3 and Y5, the contour maps between the two structural properties, the interstrand distance (d_{strand}) and the native intersheet hydrophobic contacts were computed and the results are shown in Figure 9. It is observed that, for the SH2-ST2 and SH2-ST3 models, the loss of the intersheet hydrophobic contacts is associated with the separation of the β-strands, resulting in the unstable and disordered structural organisations. In contrast, the SH2-ST4 and SH2-ST5 models tend to form a stable cluster by maintaining the stable d_{strand} and the native intersheet hydrophobic contacts during the entire simulation courses, indicating that the hydrophobic steric zipper at the sheet–sheet interface is important in

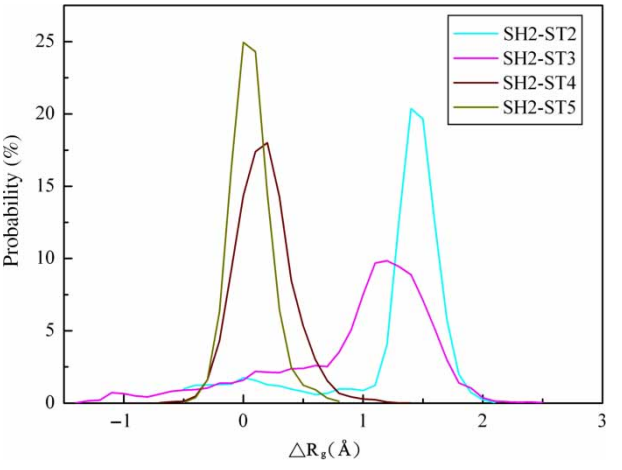

Figure 8. The distributions of ΔR_g of the steric zipper involving the V1, I3 and Y5 side chains are calculated as $\Delta R_g = R_{gi} - R_{g0}$, where R_{gi} and R_{g0} are the R_g of the hydrophobic V1, I3 and Y5 side chains during the simulation and in the crystal structure, respectively.

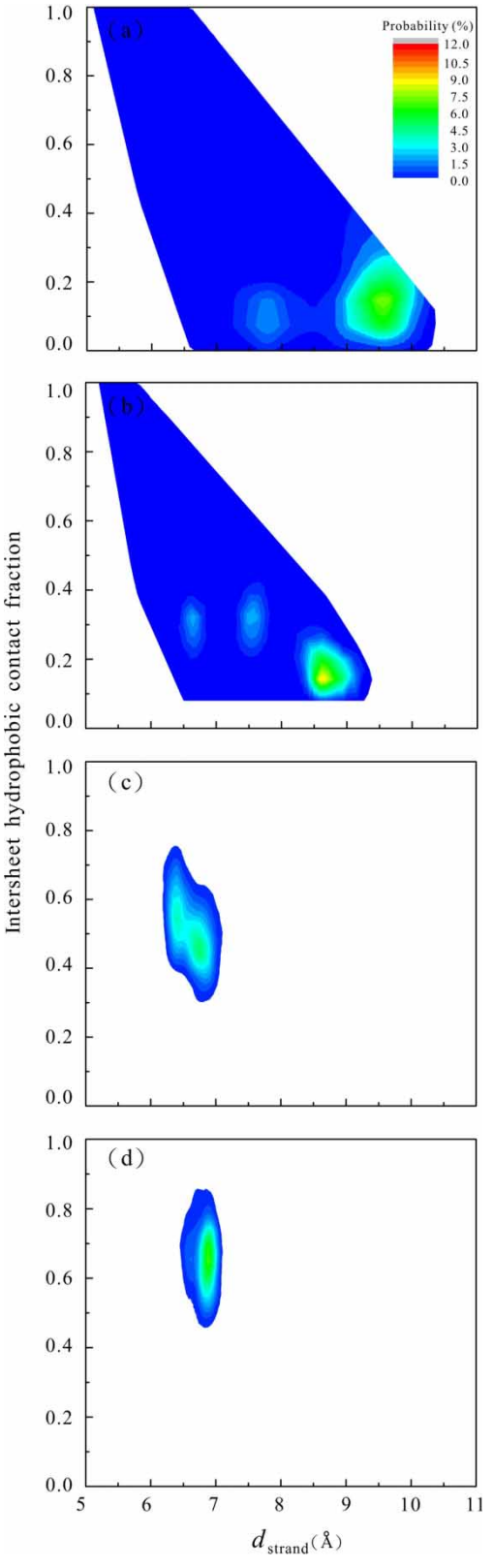

Figure 9. Contour maps between the intersheet hydrophobic contact fraction and interstrand distance (d_{strand}) for the (a) SH2-ST2, (b) SH2-ST3, (c) SH2-ST4 and (d) SH2-ST5 models.

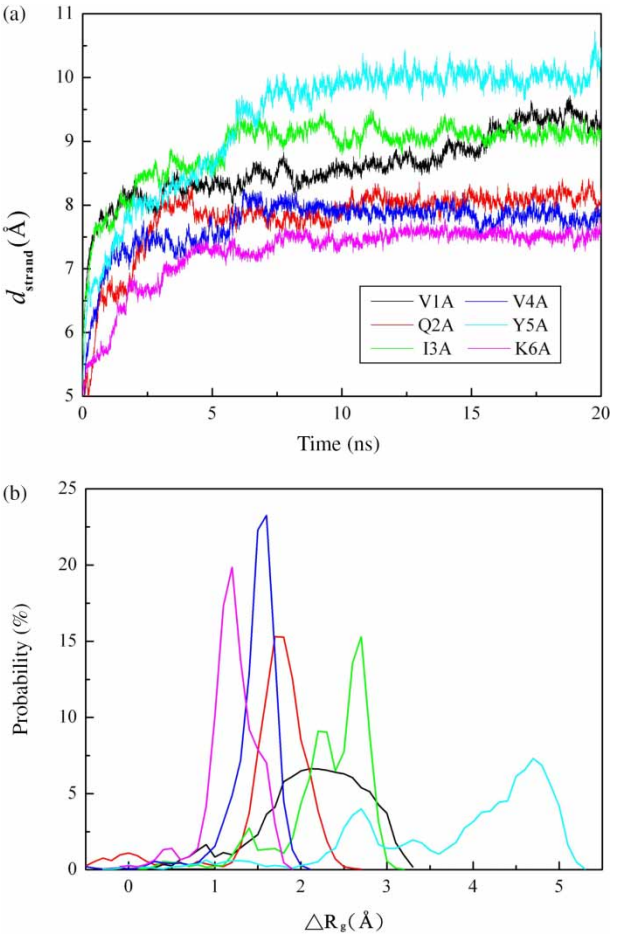

Figure 10. (a) Interstrand distance (d_{strand}) and (b) distributions of ΔR_g of the steric zipper involved the side chains of residues 1, 3 and 5 during the 20 ns MD simulations for the mutant models.

holding the neighbouring β-sheet layers together. Our results are consistent with the recent Monte Carlo simulations towards the tau fragment AcPHF6, showing that larger aggregates are all consisted of two twisted β-sheet layers packed against each other with the hydrophobic side chains at the sheet–sheet interface [46]. The importance of the sheet–sheet interactions in maintaining the entire oligomeric stability has also been described in several previous theoretical studies. For example, previous MD study of the structural stability and dynamics of various GNNQQNY oligomers [45] has indicated that a dry polar steric zipper via the self-complementing side chain contacts (i.e. N2–N6, Q4–Q4 and N6–N2) provides a major driving force to promote the association of antiparallel β-sheet layers. In addition, the hydrophobic side-chain interactions of Aβ40 (Aβ42) are largely involved in the sheet–sheet interface, forming the self-complementing tight steric zipper [49].

3.4 The stability of the VQIVYK mutants: sequence effects

To investigate the effects of mutants on the structural stability of VQIVYK oligomers, each of the residues was substituted by Ala. All of these mutant systems were built based on the SH2-ST5 model. Figure 10(a) and (b) presents the d_{strand} and ΔR_g of the steric zipper involving residues 1, 3 and 5, respectively, for these mutants. In Figure 10(a), the results suggest that all mutants are more structurally unstable relative to the wild-type SH2-ST5 model, particularly for the cases of V1A, I3A and Y5A. In contrast, the Q2A, V4A and K6A mutants exhibit little effect on the structural stability of the VQIVYK oligomers as reflected by the lower d_{strand} than those of the V1A, I3A and Y5A mutants. Figure 10(b) shows that Q2A, V4A and K6A mutants do not affect the compactness of the steric zipper interfaces, whereas the V1A, I3A and Y5A mutants dramatically destabilise the steric zipper interfaces. It can be attributed to the fact that the side chains of Q2, V4 and K6 are oriented towards the peptide–water interface and the substitutions by Ala at these positions do not directly alter the hydrophobic steric zipper between the two neighbouring β-sheet layers. However, the side chains of V1, I3 and Y5 are pointed towards the interface between the two neighbouring β-sheet layers to form a hydrophobic steric zipper (Figure 1). Thus, the substitution of these residues to Ala would directly destroy the structural organisation of the steric zipper, resulting in an unstable oligomeric organisation. Previous MD study of the GNNQQNY peptide also reported that the residue substitutions at the sheet–sheet interface would cause larger destabilisation than those oriented towards the peptide–water interface [45]. To further investigate the mutant effects of V1A, I3A and Y5A, the contour maps between the d_{strand} and the native intersheet hydrophobic contacts are presented in Figure 11. It is clear that the collapses of the hydrophobic interactions between the two β-sheet layers are associated with the disassociation of the adjacent β-strands, leading to the destruction of the entire oligomeric structures.

Among these mutants, Y5A exhibits the highest ability to destabilise the structural organisation due to the lack of the π–π stacking interaction between the adjacent β-strands and the loss of the hydrophobic interactions between the neighbouring β-sheet layers. These results are consistent with the previous experimental results, showing that the substitution of Tyr by Ala significantly decreases the polymerisation rate of VQIVYK peptides [17] and that the substitution of Tyr by Gly directly abolishes the VQIVYK aggregations [50]. The importance of the π–π stacking interaction has also been demonstrated in many other amyloid-forming peptides [51,52].

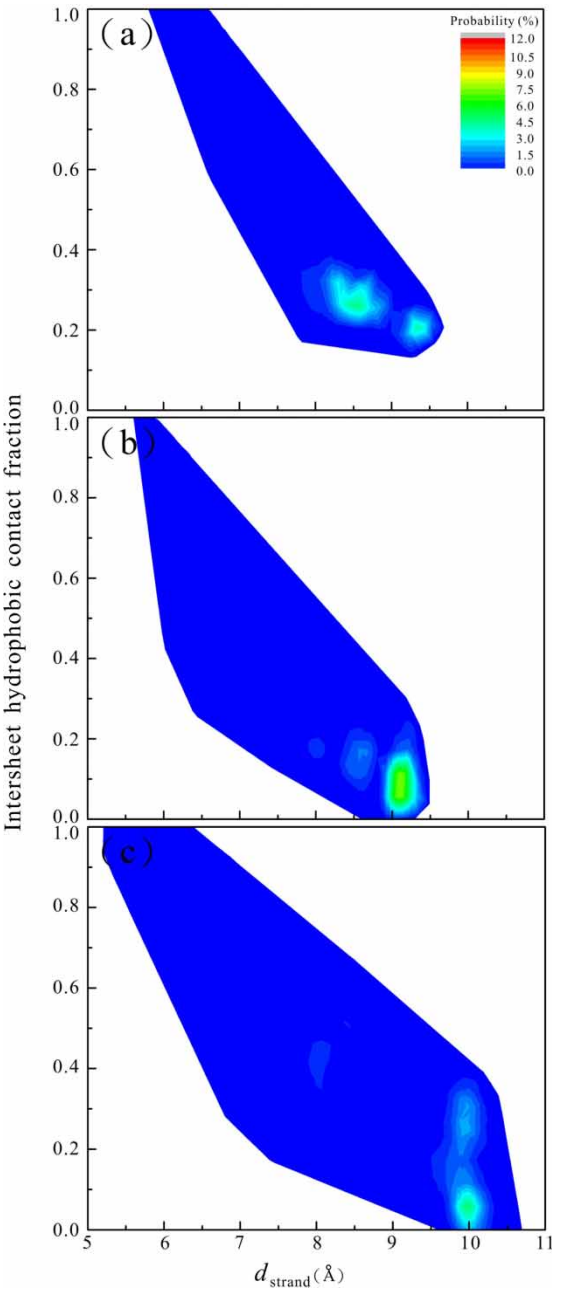

Figure 11. Contour maps between the intersheet hydrophobic contact fraction and the interstrand distance (d_{strand}) for the (a) V1A, (b) I3A and (c) Y5A mutants.

3.5 Common structural property of amyloid fibrils: twisted β-strand

It is well accepted that twisted β-strand is the common structural property of amyloid fibrils [53], although the crystal structure exhibits a planar structure [22,23]. Several theoretical studies have reported a common twisted β-strand pattern for many amyloidogenic peptides [24,28,48,54–62], with the twisted angles ranged from 9° to 20°. To gain insights into this structural feature of the

models emerged from the current MD simulations, the twisted angles between two adjacent β-strands of the VQIVYK oligomers were analysed and the results are presented in Table 2. The twisted angles of the two adjacent β-strands follow the order of SH1-ST2 > SH1-ST3 > SH1-ST4 > SH1-ST5 in the one-sheet models and of SH2-ST2 > SH2-ST3 > SH2-ST4 > SH2-ST5 in the two-sheet models, suggesting that the twisted angle between two adjacent β-strands is size dependent. Our results are consistent with the previous observation, showing that the β-sheets with few strands tend to be associated with larger twisted angles than those containing a large number of strands in native proteins [63]. Along these lines, it is expected that the twisted angles should be relatively small in amyloid fibrils, as supported by the data from the cryo-electron microscopy experiments for insulin fibrils (twisted angle 1.5°–2.5°) [64] and the TEM experiments on fibrils of rationally designed peptides (twisted angle 1°–3°) [65]. However, our simulation results show that the averaged twisted angles between two adjacent β-strands of the stable VQIVYK oligomers, such as SH2-ST4 and SH2-ST5, are comparatively large (23.4°–26.6°). It can be attributed to the fact that twisting between two adjacent β-strands optimises side-chain packing, which may reduce the K6–K6 repulsive interactions between two adjacent β-strands and generate more favourable electrostatic interactions between K6 and C-terminus. Previous MD study has also reported a large averaged twisted angle of 20° for the amyloidogenic peptide DFNKF due to the optimisation of the electrostatic interactions between the charged side chains and the termini [48].

4. Conclusions

Previous experiments using transgenic mice models have reported that soluble aggregates of tau rather than NFTs might cause neurodegeneration [66–68], which has brought up the possibility of using the oligomeric forms as drug targets. Moreover, it has been hypothesised that the formation of PHFs arising from short hexapeptide motifs in the third repeat of tau, ^{306}VQIVYK^{311}, is critical for tau polymerisation [13–16]. Recently, the amyloid-like structure of the VQIVYK peptide has been determined by X-ray microcrystallography [23], and is thought to be a good model for studying the early stage of the aggregation process. In this study, several MD simulations with all-atom explicit water were conducted to investigate the structural stability and aggregation behaviour of the VQIVYK peptide and its single alanine replacement mutations to gain insights into the possible mechanism of fibrillogenesis.

Table 2. Averaged twisted angles of two adjacent β-strands of the VQIVYK oligomers.

Models	Averaged twisted angle (°)
SH1-ST2	96.5 ± 9.3
SH1-ST3	86.8 ± 5.9
SH1-ST4	71.1 ± 5.8
SH1-ST5	47.9 ± 6.3
SH2-ST2	69.1 ± 3.8
SH2-ST3	58.5 ± 2.9
SH2-ST4	25.2 ± 1.4
SH2-ST5	24.7 ± 1.3

The major findings of this study can be summarised as follows: (i) extra β-strands or β-sheet layers delay the progressive loss of the β-structural organisation and therefore increase the structural stability of the VQIVYK oligomers; (ii) the van der Waals interactions between Q2 side chains, the π–π stacking interaction between the Y5 aromatic rings and the electrostatic interaction between K6 and C-terminus play an important role in associating and stabilising the VQIVYK oligomers within the same β-sheet layer; (iii) the interactions involving Y5 and K6 play a critical role in initiating the VQIVYK oligomerisation; (iv) the hydrophobic steric zipper interactions involving V1, I3 and Y5 between the sheet–sheet interface contribute significantly to maintain the entire oligomeric structures; (v) a single alanine substitution at the position of V1, I3 and Y5 remarkably disrupts the hydrophobic steric zipper; and (vi) the twisted angles between the adjacent β-strands within the same β-sheet layer are size dependent.

Furthermore, our simulation results suggest that Y5 is the most important residue for both β-strand stacking and sheet–sheet association due to the fact that the aromatic rings provide interstrand π–π stacking and the intersheet hydrophobic interactions to maintain the entire VQIVYK oligomers. Our mutant simulations in the absence of the Y5 ring showed decreased stability. Previously, Gazit [51] has reported that the aromatic residues such as Phe, Tyr and Trp were frequently found in a variety of amyloid-related peptides, supporting the significant role of aromatic residues in amyloid fibril formation. Moreover, Makin and co-workers [69] have indicated that aromatic residues are important for fibril formation due to π–π stacking and that highly conserved aromatic residues provide strong entropic contributions to stabilise existing oligomers/fibrils. Take together, our results imply that designing an inhibitor to break the interstrand π–π stacking interaction or the intersheet hydrophobic interactions may be a possible strategy to inhibit the formation of the early aggregates of tau protein. Such strategy has been recently reviewed by Bulic et al. [70]. The present results not only provide atomic insights into amyloid formation, but are also helpful for designing new or modified inhibitors to prevent fibril formation of the VQIVYK peptide from tau protein.

Acknowledgements

The authors gratefully acknowledge the financial support from the National Science Council of Taiwan (Project numbers: NSC-96-2221-E-027-045-MY3, NSC-96-2628-E-027-002-MY3 and NSC-98-2622-E-027-023-CC3), the Institute of Nuclear Energy Research of Taiwan (Project number: 992001INER072), and the National Taipei University of Technology and Taipei Medical University (Project number: NTUT-TMU-98-02).

References

[1] D.J. Selkoe, *The origins of Alzheimer disease: A is for amyloid*, JAMA 283 (2000), pp. 1615–1617.

[2] M. Goedert, G. Spillantini, N.J. Cairns, and R.A. Crowther, *Tau proteins of Alzheimer paired helical filaments: Abnormal phosphorylation of all six brain isoforms*, Neuron 8 (1992), pp. 159–168.

[3] A. Alonso, T. Zaidi, M. Novak, I. Grundke-Iqbal, and K. Iqbal, *Hyperphosphorylation induces self-assembly of tau into tangles of paired helical filaments/straight filaments*, Proc. Natl Acad. Sci. USA 98 (2001), pp. 6923–6928.

[4] M. Necula and J. Kuret, *Pseudophosphorylation and glycation of tau protein enhance but do not trigger fibrillization* in vitro, J. Biol. Chem. 279 (2004), pp. 49694–49703.

[5] A. Schneider, J. Biernat, M. von Bergen, E. Mandelkow, and E.M. Mandelkow, *Phosphorylation that detaches tau protein from microtubules (Ser-262, Ser-214) also protects it against aggregation into Alzheimer paired helical filaments*, Biochemistry 38 (1999), pp. 3549–3558.

[6] D.W. Cleveland, S.Y. Hwo, and M.W. Kirschner, *Physical and chemical properties of purified tau factor and the role of tau in microtubule assembly*, J. Mol. Biol. 116 (1977), pp. 227–247.

[7] S. Jeganathan, M. von Bergen, H. Brutlach, H.J. Steinhoff, and E. Mandelkow, *Global hairpin folding of tau in solution*, Biochemistry 45 (2006), pp. 2283–2293.

[8] O. Schweers, E. Schönbrunn-Hanebeck, A. Marx, and E. Mandelkow, *Structural studies of tau protein and Alzheimer paired helical filaments show no evidence for beta-structure*, J. Biol. Chem. 269 (1994), pp. 24290–24297.

[9] M. von Bergen, S. Barghorn, J. Biernat, E.M. Mandelkow, and E. Mandelkow, *Tau aggregation is driven by a transition from random coil to beta sheet structure*, Biochim. Biophys. Acta 1739 (2005), pp. 158–166.

[10] C.M. Wischik, M. Novak, H.C. Thogersen, P.C. Edwards, M.J. Runswick, R. Jakes, J.E. Walker, C. Milstein, M. Roth, and A. Klug, *Isolation of a fragment of tau derived from the core of the paired helical filament of Alzheimer disease*, Proc. Natl Acad. Sci. USA 85 (1988), pp. 4506–4510.

[11] K. Minoura, T.M. Yao, K. Tomoo, M. Sumida, M. Sasaki, T. Taniguchi, and T. Ishida, *Different associational and conformational behaviors between the second and third repeat fragments in the tau microtubule-binding domain*, Eur. J. Biochem. 271 (2004), pp. 545–552.

[12] H. Wille, G. Drewes, J. Biernat, E.M. Mandelkow, and E. Mandelkow, *Alzheimer-like paired helical filaments and antiparallel dimers formed from microtubule-associated protein tau* in vitro, J. Cell Biol. 118 (1992), pp. 573–584.

[13] M. von Bergen, P. Friedhoff, J. Biernat, J. Heberle, E.-M. Mandelkow, and E. Mandelkow, *Assembly of tau protein into Alzheimer paired helical filaments depends on a local sequence motif ((306)VQIVYK(311)) forming beta structure*, Proc. Natl Acad. Sci. USA 97 (2000), pp. 5129–5134.

[14] M. von Bergen, S. Barghorn, L. Li, A. Marx, J. Biernat, E.-M. Mandelkow, and E. Mandelkow, *Mutations of tau protein in frontotemporal dementia promote aggregation of paired helical filaments by enhancing local beta-structure*, J. Biol. Chem. 276 (2001), pp. 48165–48174.

[15] S. Barghorn, Q. Zheng-Fischhofer, M. Ackmann, J. Biernat, M. von Bergen, E.-M. Mandelkow, and E. Mandelkow, *Structure, microtubule interactions, and paired helical filament aggregation by tau mutants of frontotemporal dementias*, Biochemistry 39 (2000), pp. 11714–11721.

[16] S. Barghorn and E. Mandelkow, *Toward a unified scheme for the aggregation of tau into Alzheimer paired helical filaments*, Biochemistry 41 (2002), pp. 14885–14896.

[17] W.J. Goux, L. Kopplin, A.D. Nguyen, K. Leak, M. Rutkofsky, V.D. Shanmuganandam, D. Sharma, H. Inouye, and D.A. Kirschner, *The formation of straight and twisted filaments from short tau peptides*, J. Biol. Chem. 279 (2004), pp. 26868–26875.

[18] C.M. Dobson, *Structural biology: Prying into prions*, Nature 435 (2005), pp. 747–749.

[19] O.S. Makin and L.C. Serpell, *X-ray diffraction studies of amyloid structure*, Methods Mol. Biol. 299 (2005), pp. 67–80.

[20] O.S. Makin and L.C. Serpell, *Structures for amyloid fibrils*, FEBS J. 272 (2005), pp. 5950–5961.

[21] D. Thirumalai, D.K. Klimov, and R.I. Dima, *Emerging ideas on the molecular basis of protein and peptide aggregation*, Curr. Opin. Struct. Biol. 13 (2003), pp. 146–159.

[22] R. Nelson, M.R. Sawaya, M. Balbirnie, A.O. Madsen, C. Riekel, R. Grothe, and D. Eisenberg, *Structure of the cross-beta spine of amyloid-like fibrils*, Nature 435 (2005), pp. 773–778.

[23] M.R. Sawaya, S. Sambashivan, R. Nelson, M.I. Ivanova, S.A. Sievers, M.I. Apostol, M.J. Thompson, M. Balbirnie, J.J. Wiltzius, H.T. McFarlane, A.Ø. Madsen, C. Riekel, and D. Eisenberg, *Atomic structures of amyloid cross-beta spines reveal varied steric zippers*, Nature 447 (2007), pp. 453–457.

[24] B. Ma and R. Nussinov, *Stabilities and conformations of Alzheimer's beta-amyloid peptide oligomers (Abeta 16–22, Abeta 16–35, and Abeta 10–35): Sequence effects*, Proc. Natl Acad. Sci. USA 99 (2002), pp. 14126–14131.

[25] I. Daidone, F. Simona, D. Roccatano, R.A. Broglia, G. Tiana, G. Colombo, and A. Di Nola, *Beta-hairpin conformation of fibrillogenic peptides: Structure and alpha–beta transition mechanism revealed by molecular dynamics simulations*, Proteins 57 (2004), pp. 198–204.

[26] J. Gsponer, U. Haberthur, and A. Caflisch, *The role of side-chain interactions in the early steps of aggregation: Molecular dynamics simulations of an amyloid-forming peptide from the yeast prion Sup35*, Proc. Natl Acad. Sci. USA 100 (2003), pp. 5154–5159.

[27] G. Colombo, I. Daidone, E. Gazit, A. Amadei, and A. Di Nola, *Molecular dynamics simulation of the aggregation of the core-recognition motif of the islet amyloid polypeptide in explicit water*, Proteins 59 (2005), pp. 519–527.

[28] A. Melquiond, G. Boucher, N. Mousseau, and P. Derreumaux, *Following the aggregation of amyloid-forming peptides by computer simulations*, J. Chem. Phys. 122 (2005), p. 174904.

[29] N. Mousseau and P. Derreumaux, *Exploring the early steps of amyloid peptide aggregation by computers*, Acc. Chem. Res. 38 (2005), pp. 885–891.

[30] S. Gnanakaran, R. Nussinov, and A.E. Garcia, *Atomic-level description of amyloid beta-dimer formation*, J. Am. Chem. Soc. 128 (2006), pp. 2158–2159.

[31] H.D. Nguyen and C.K. Hall, *Spontaneous fibril formation by polyalanines; Discontinuous molecular dynamics simulations*, J. Am. Chem. Soc. 128 (2006), pp. 1890–1901.

[32] D. Zanuy and R. Nussinov, *The sequence dependence of fiber organization. A comparative molecular dynamics study of the islet amyloid polypeptide segments 22–27 and 22–29*, J. Mol. Biol. 329 (2003), pp. 565–584.

[33] D.K. Klimov, J.E. Straub, and D. Thirumalai, *Aqueous urea solution destabilizes Abeta(16–22) oligomers*, Proc. Natl Acad. Sci. USA 101 (2004), pp. 14760–14765.

[34] H.-H. Tsai (Gavin), D. Zanuy, N. Haspel, K. Gunasekaran, B. Ma, C.-J. Tsai, and R. Nussinov, *The stability and dynamics of the human calcitonin amyloid peptide DFNKF*, Biophys. J. 87 (2004), pp. 146–158.

[35] D. Zanuy, N. Haspel, H.H. Tsai, B. Ma, K. Gunasekaran, H.J. Wolfson, and R. Nussinov, *Side chain interactions determine the amyloid organization: A single layer beta-sheet molecular structure of the calcitonin peptide segment 15–19*, Phys. Biol. 1 (2004), pp. 89–99.

[36] D. Zanuy, Y. Porat, E. Gazit, and R. Nussinov, *Peptide sequence and amyloid formation; Molecular simulations and experimental*

study of a human islet amyloid polypeptide fragment and its analogs, Structure 12 (2004), pp. 439–455.
[37] M. López de la Paz, G.M. de Mori, L. Serrano, and G. Colombo, *Sequence dependence of amyloid fibril formation: Insights from molecular dynamics simulations*, J. Mol. Biol. 349 (2005), pp. 583–596.
[38] G.G. Tartaglia, A. Cavalli, R. Pellarin, and A. Caflisch, *Prediction of aggregation rate and aggregation-prone segments in polypeptide sequences*, Protein Sci. 14 (2005), pp. 2723–2734.
[39] L.-K. Chang, J.-H. Zhao, H.-L. Liu, K.-T. Liu, J.-T. Chen, W.-B. Tsai, and Y. Ho, *Molecular dynamics simulations to investigate the structural stability and aggregation behavior of the GGVVIA oligomers derived from amyloid β peptide*, J. Biomol. Struct. Dyn. 26 (2009), pp. 731–740.
[40] H.C. Andersen, *RATTLE: A 'velocity' version of the shake algorithm for molecular dynamics calculations*, J. Comput. Phys. 52 (1983), pp. 24–34.
[41] H.H. Tsai, M. Reches, C.J. Tsai, K. Gunasekaran, E. Gazit, and R. Nussinov, *Energy landscape of amyloidogenic peptide oligomerization by parallel-tempering molecular dynamics simulation: Significant role of Asn ladder*, Proc. Natl Acad. Sci. USA 102 (2005), pp. 8174–8179.
[42] D. Zanuy, C. Alemán, and S. Muñoz-Guerra, *A molecular dynamics study in chloroform solution of the stoichiometric complex formed by poly(alpha, L-glutamate) and octylmethylammonium ions*, Biopolymers 63 (2002), pp. 151–162.
[43] C. Aleman and D. Zanuy, *Binding in complex ionic systems: Anticooperative effects in systems stabilized by electrostatic interactions*, Chem. Phys. Lett. 343 (2001), pp. 390–396.
[44] U. Samanta, D. Pal, and P. Chakrabarti, *Packing of aromatic rings against tryptophan residues in proteins*, Acta Crystallogr. D55 (1999), pp. 1421–1427.
[45] J. Zheng, B. Ma, C.J. Tsai, and R. Nussinov, *Structural stability and dynamics of an amyloid-forming peptide GNNQQNY from the yeast prion sup-35*, Biophys. J. 91 (2006), pp. 824–833.
[46] D.W. Li, S. Mohanty, A. Irbäck, and S. Huo, *Formation and growth of oligomers: A Monte Carlo study of an amyloid tau fragment*, PLoS Comput. Biol. 4 (2008), pp. 1–12.
[47] R. Bhattacharyya, U. Samanta, and P. Chakrabarti, *Aromatic–aromatic interactions in and around alpha-helices*, Protein Eng. 15 (2002), pp. 91–100.
[48] N. Haspel, D. Zanuy, B. Ma, H. Wolfson, and R. Nussinov, *A comparative study of amyloid fibril formation by residues 15–19 of the human calcitonin hormone: A single beta-sheet model with a small hydrophobic core*, J. Mol. Biol. 345 (2005), pp. 1213–1227.
[49] N.V. Buchete, R. Tycko, and G. Hummer, *Molecular dynamics simulations of Alzheimer's beta-amyloid protofilaments*, J. Mol. Biol. 353 (2005), pp. 804–821.
[50] F.A. Rojas Quijano, D. Morrow, B.M. Wise, F.L. Brancia, and W.J. Goux, *Prediction of nucleating sequences from amyloidogenic propensities of tau-related peptides*, Biochemistry 45 (2006), pp. 4638–4652.
[51] E. Gazit, *A possible role for pi-stacking in the self-assembly of amyloid fibrils*, FASEB J. 16 (2002), pp. 77–83.
[52] E. Gazit, *Mechanisms of amyloid fibril self-assembly and inhibition. Model short peptides as a key research tool*, FEBS J. 272 (2005), pp. 5971–5978.
[53] J. Zheng, B. Ma, and R. Nussinov, *Consensus features in amyloid fibrils: Sheet–sheet recognition via a (polar or nonpolar) zipper structure*, Phys. Biol. 3 (2006), pp. P1–P4.
[54] D.K. Klimov and D. Thirumalai, *Dissecting the assembly of Ab16–22 amyloid peptides into antiparallel beta-sheets*, Structure 11 (2003), pp. 295–307.
[55] D. Zanuy, B. Ma, and R. Nussinov, *Short peptide amyloid organization: Stabilities and conformations of the islet amyloid peptide NFGAIL*, Biophys. J. 84 (2003), pp. 1884–1994.
[56] C. Wu, H. Lei, and Y. Duan, *The role of Phe in the formation of well-ordered oligomers of amyloidogenic hexapeptide (NFGAIL) observed in molecular dynamics simulations with explicit solvent*, Biophys. J. 88 (2005), pp. 2897–2906.
[57] A. Baumketner and J.E. Shea, *Free energy landscapes for amyloidogenic tetrapeptides dimerization*, Biophys. J. 89 (2005), pp. 1493–1503.
[58] G. Wei, N. Mousseau, and P. Derreumaux, *Sampling the self-assembly pathways of KFFE hexamers*, Biophys. J. 87 (2004), pp. 3648–3656.
[59] H. Lei, C. Wu, Z. Wang, and Y. Duan, *Molecular dynamics simulations and free energy analyses on the dimer formation of an amyloidogenic heptapeptide from human beta2-microglobulin: Implication for the protofibril structure*, J. Mol. Biol. 356 (2006), pp. 1049–1063.
[60] A. Baumketner, S.L. Bernstein, T. Wyttenbach, N.D. Lazo, D.B. Teplow, M.T. Bowers, and J.E. Shea, *Structure of the 21–30 fragment of amyloid beta-protein*, Protein Sci. 15 (2006), pp. 1239–1247.
[61] L. Esposito, C. Pedone, and L. Vitagliano, *Molecular dynamics analyses of cross-beta-spine steric zipper models: Beta-sheet twisting and aggregation*, Proc. Natl Acad. Sci. USA 103 (2006), pp. 11533–11538.
[62] A. De Simone, C. Pedone, and L. Vitagliano, *Structure, dynamics, and stability of assemblies of the human prion fragment SNQNNF*, Biochem. Biophys. Res. Commun. 366 (2008), pp. 800–806.
[63] J.S. Richardson, *The anatomy and taxonomy of protein structure*, Adv. Protein Chem. 34 (1981), pp. 167–339.
[64] J.L. Jimenez, E.J. Nettleton, M. Bouchard, C.V. Robinson, C.M. Dobson, and H.R. Saibil, *The protofilament structure of insulin amyloid fibrils*, Proc. Natl Acad. Sci. USA 99 (2002), pp. 9196–9201.
[65] A. Aggeli, I.A. Nyrkova, M. Bell, R. Harding, L. Carrick, T.C. McLeish, A.N. Semenov, and N. Boden, *Hierarchical self-assembly of chiral rod-like molecules as a model for peptide beta-sheet tapes, ribbons, fibrils, and fibers*, Proc. Natl Acad. Sci. USA 98 (2001), pp. 11857–11862.
[66] S. Le Corre, H.W. Klafki, N. Plesnila, G. Hubinger, A. Obermeier, H. Sahagún, B. Monse, P. Seneci, J. Lewis, J. Eriksen, C. Zehr, M. Yue, E. McGowan, D.W. Dickson, M. Hutton, and H.M. Roder, *An inhibitor of tau hyperphosphorylation prevents severe motor impairments in tau transgenic mice*, Proc. Natl Acad. Sci. USA 103 (2006), pp. 9673–9678.
[67] K. Santacruz, J. Lewis, T. Spires, J. Paulson, L. Kotilinek, M. Ingelsson, A. Guimaraes, M. DeTure, M. Ramsden, E. McGowan, C. Forster, M. Yue, J. Orne, C. Janus, A. Mariash, M. Kuskowski, B. Hyman, M. Hutton, and K.H. Ashe, *Tau suppression in a neurodegenerative mouse model improves memory function*, Science 309 (2005), pp. 476–481.
[68] J.Q. Trojanowski and V.M. Lee, *Pathological tau: A loss of normal function or a gain in toxicity?* Nat. Neurosci. 8 (2005), pp. 1136–1137.
[69] O.S. Makin, E. Atkins, P. Sikorski, J. Johansson, and L.C. Serpell, *Molecular basis for amyloid fibril formation and stability*, Proc. Natl Acad. Sci. USA 102 (2005), pp. 315–320.
[70] B. Bulic, M. Pickhardt, B. Schmidt, E.M. Mandelkow, H. Waldmann, and E. Mandelkow, *Development of tau aggregation inhibitors for Alzheimer's disease*, Angew. Chem. Int. Ed. Engl. 48 (2009), pp. 1740–1752.